

# Electrically Driven Hot-Carrier Generation and Above-Threshold Light Emission in Plasmonic Tunnel Junctions

Longji Cui, Yunxuan Zhu, Mahdiyeh Abbasi, Arash Ahmadvand, Burak Gerislioglu, Peter Nordlander, and Douglas Natelson\*

Cite This: *Nano Lett.* 2020, 20, 6067–6075

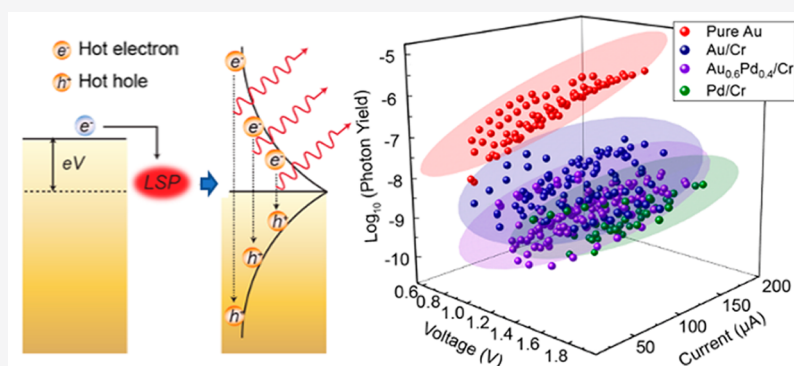
Read Online

ACCESS |

Metrics & More

Article Recommendations

Supporting Information



**ABSTRACT:** Above-threshold light emission from plasmonic tunnel junctions, when emitted photons have energies significantly higher than the energy scale of incident electrons, has attracted much recent interest in nano-optics, while the underlying physics remains elusive. We examine above-threshold light emission in electromigrated tunnel junctions. Our measurements over a large ensemble of devices demonstrate a giant ( $\sim 10^4$ ) material-dependent photon yield (emitted photons per incident electrons). This dramatic effect cannot be explained only by the radiative field enhancement due to localized plasmons in the tunneling gap. Emission is well described by a Boltzmann spectrum with an effective temperature exceeding 2000 K, coupled to a plasmon-modified photonic density of states. The effective temperature is approximately linear in the applied bias, consistent with a suggested theoretical model describing hot-carrier dynamics driven by nonradiative decay of electrically excited localized plasmons. Electrically generated hot carriers and nontraditional light emission could open avenues for active photochemistry, optoelectronics, and quantum optics.

**KEYWORDS:** Plasmonics, tunnel junction, light emission, hot-carrier dynamics

## INTRODUCTION

Localized surface plasmons (LSPs) in metal nanostructures are of great current interest for their role in generating non-equilibrium hot carriers for photochemistry,<sup>1–3</sup> photodetection,<sup>4,5</sup> photoluminescence,<sup>6</sup> and photovoltaics.<sup>7,8</sup> LSPs and plasmon-induced hot-carrier dynamics can be driven either by optical illumination or electrically via inelastic tunneling. In electrically driven tunnel junctions, plasmon-enhanced light emission has been found promising for a variety of technologies that require efficient optoelectronic integration and conversion at the nanoscale.<sup>9–16</sup> Radiative decay of inelastically excited LSPs has been recognized as a dominant light emission mechanism,<sup>17</sup> leading to broadband emission at photon energies  $\hbar\omega$  less than the “single-electron” energy scale corresponding to the applied voltage (i.e.,  $\hbar\omega \leq eV$ ).<sup>9,13,16,18–21</sup> Numerous efforts<sup>9,13,16,18</sup> have focused on optimizing plasmonic excitations of metallic nanostructures to improve light emission efficiency. Interestingly, a number of pioneering works<sup>22–27</sup> performed by scanning tunneling

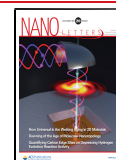
microscopy and nanofabricated tunnel junctions have reported the observation of above-threshold light emission, where emitted photons have energies extending to 2 eV or even 3 eV in contradiction with a simple single-electron picture of electrically driven plasmonic excitation and decay.

In contrast to below-threshold light emission, above-threshold light emission ( $\hbar\omega > eV$ ) requires multielectron processes. One possible mechanism is based on blackbody radiation of the hot-electron gas formed in the drain electrode by electrons that elastically tunnel through the junction.<sup>22,25</sup> In this physical picture, tunneling electrons can thermalize rapidly via inelastic electron–electron scattering, faster than their

Received: May 19, 2020

Revised: June 20, 2020

Published: June 22, 2020



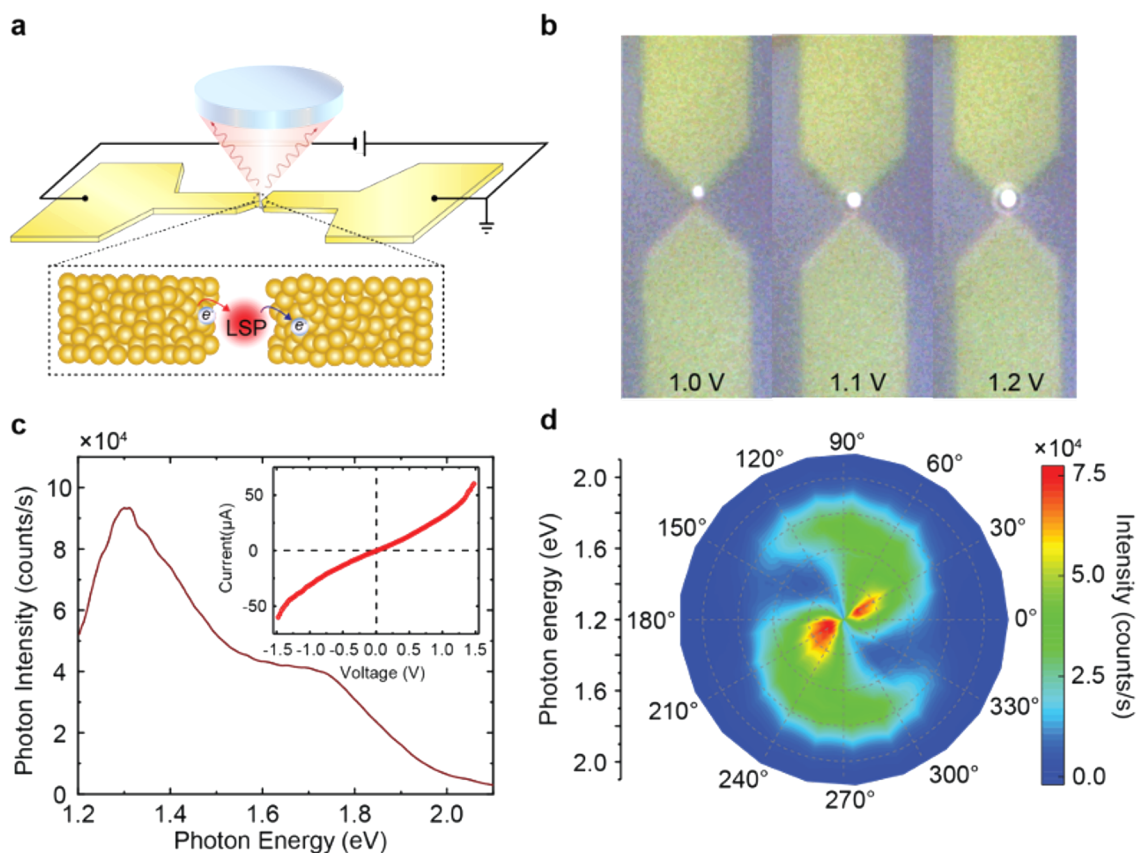


**Figure 1.** Experimental strategy for measuring light emission in electrically driven tunnel junctions. (a) Schematics of the experimental setup capable of simultaneous electrical transport and optical spectroscopy measurements. LSP denotes the localized surface plasmons excited by the inelastic tunneling electrons. (b) Wide-field CCD imaging of an Au light-emitting tunnel junction operating under bias from 1.0 to 1.2 V. A weak white light source is applied to illuminate the device structure. (c) Measured light emission spectrum of the Au tunnel junction at 1.0 V. Inset shows the dc  $I$ - $V$  characteristics of the junction. (d) Polarization-dependent spectral light emission contour plot for the operating tunnel junction in (c) at 1.0 V;  $0^\circ$  and  $90^\circ$  denotes the polarization across and transverse to the tunnel junction, respectively. The radial coordinate indicates photon energy, while the color scale gives the detected intensity.

energy can be coupled to the lattice via electron–phonon scattering. The result is a hot electron gas on top of a background of cold carriers with the hot electrons distribution characterized by an effective temperature set by the dissipated electrical power (Joule heating) and electronic transport of heat. That effective temperature can be much higher than the equilibrium lattice temperature. The emission spectrum of this hot electron gas reflects the plasmon-modified local photon density of states rather than the free-space density of states. Other multielectron mechanisms<sup>23,26–29</sup> have also been proposed under which coherent interactions between electrons, either through Auger-like processes or mediated by plasmonic excitations, could facilitate inelastic tunneling electrons gaining excess energy above  $eV$  and subsequently lead to above-threshold light emission via radiative decay of LSPs. Despite these mechanisms, it remains a great challenge to experimentally identify the physical origin of above-threshold light emission.

In this work, we perform experimental studies on light emission from tunnel junctions made of materials with differing plasmonic properties and under various electrical driving conditions. A surprisingly strong material-dependent photon yield is observed, as large as  $10^4$ -fold, which cannot be explained solely by the well-established material-dependent radiative field enhancement (proportional to the local photon density of states) due to the LSPs confined in the

subnanometer-sized tunneling gap. In pure Au junctions, nearly all emitted photons can be above threshold. We confirm that the emission spectrum is Boltzmann distributed and coupled with the junction-specific plasmon-modified photon density of states, showing that there are hot carriers described by an effective temperature much higher than the lattice temperature. In contrast to prior studies, when looking at the ensemble of junctions we find that this effective temperature is set by the bias voltage rather than dissipated electrical power. We propose a microscopic theoretical model based on hot carriers generated by nonradiative decay of inelastically excited plasmons and find it consistent with our measurements and statistical analysis over a large ensemble of devices.

## RESULTS AND DISCUSSION

Our experimental approach for measuring light emission in plasmonic tunnel junctions is illustrated in Figure 1a. We fabricated samples consisting of arrays of nanowires made of several different metallic materials (Au, Au/Cr,  $\text{Au}_{0.6}\text{Pd}_{0.4}/\text{Cr}$ , and Pd/Cr) (see Supporting Information Section 1 for the nanofabrication steps). These materials were chosen deliberately to test the role of plasmons in the emission process, as these metals range from good to poor plasmonic properties in the red part of the visible spectrum. Numerical simulation is conducted to optimize the geometry of the nanowires (600 nm long, 100 nm wide, and 18 nm thick) to obtain maximal

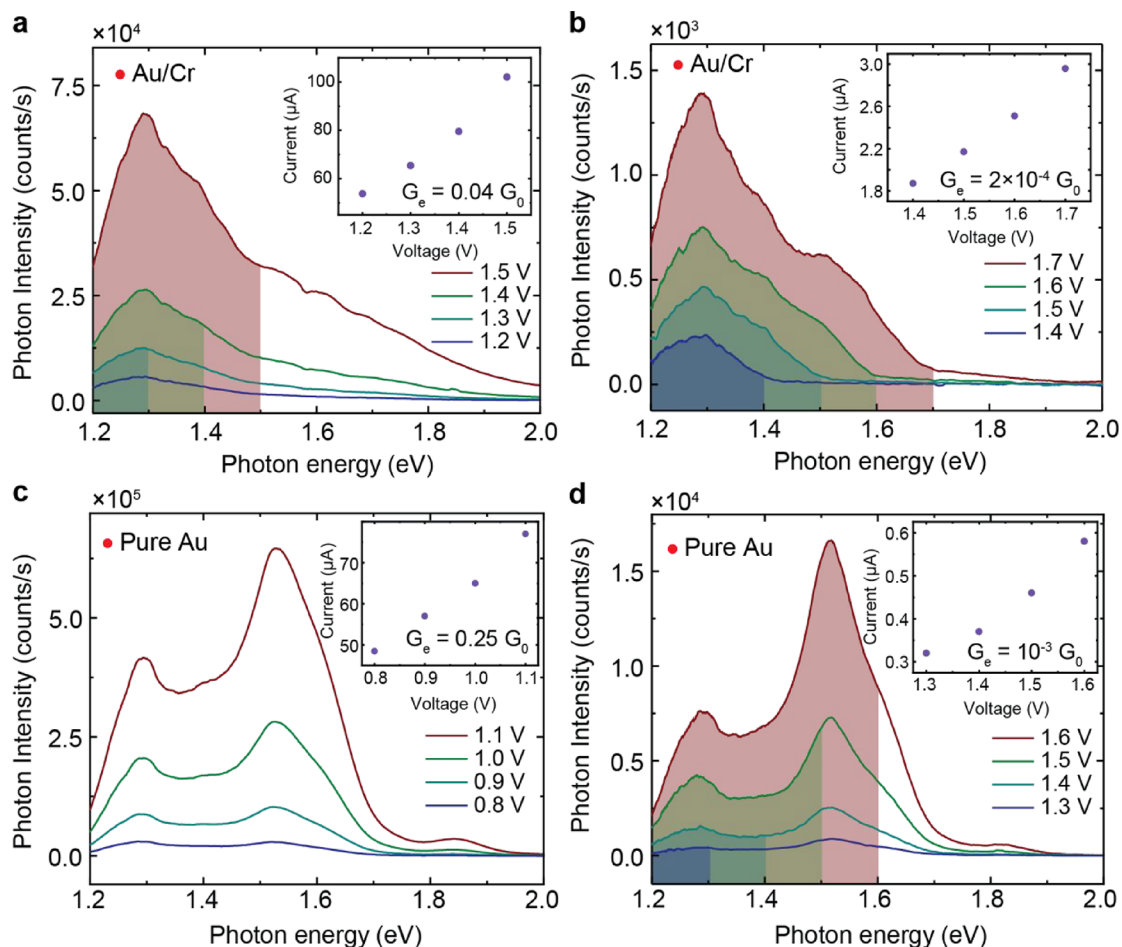


**Figure 2.** Measured above-threshold light emission in different current regimes of pure Au and Au/Cr tunnel junctions. (a) Spectral emission intensity for an Au/Cr tunnel junction in high-current regime ( $\sim 50\text{--}100\ \mu\text{A}$ ). The color-shaded regions mark the below-threshold portion of light emission with energy cutoff at  $eV$ . (b) Measured light emission spectra for the same tunnel junction in (a), but the junction is further electromigrated to form a wider tunnel gap (with lower zero-bias conductance) carrying much lower current ( $\sim 2\ \mu\text{A}$ ). The emission spectra exhibit clear-cut-off at the threshold energy, resembling below-threshold light emission. (c) Same as (a) but for a pure Au tunnel junction in high-current regime. All emitted photons have energies above the threshold. (d) The same pure Au junction is further electromigrated to form a low-current carrying device. A sizable portion of the light emission spectra still shows above-threshold photons. Insets in (a–d) show the corresponding  $I$ – $V$  measurements of each junction in different current regimes, and  $G_e$  is the zero-bias dc conductance in units of the quantum conductance ( $G_0 = 2e^2/h = 1/(12.9\ \text{k}\Omega)$ ).

plasmonic response. The ultrathin adhesion layer of Cr ( $\sim 1\ \text{nm}$ ) functions as a damping medium<sup>30,31</sup> to attenuate plasmonic resonances relative to the pure Au case. Au/Pd and Pd have poor plasmonic properties in this spectral range due to higher resistivity and interband transitions. To create a subnanometer-sized tunneling gap in the nanowire to form a tunnel junction, an electromigration break junction approach<sup>32</sup> was employed (see Supporting Information Section 2 and Figure S1 for more details). In performing light emission measurements, we applied a voltage bias  $V$  to drive electron tunneling through the junction and measured the electrical current and light emission simultaneously. To maintain high stability and cleanliness of the tunnel junctions, our experiments were performed with the substrate temperature at 5 K in high vacuum. Emitted photons from the junction were collected through free-space optics and imaged on a CCD camera/spectrometer (see Supporting Information Section 3 for the experimental setup).

As shown in Figure 1b, the wide-field light emitting images of the tunnel junction operating under increasing voltage bias  $V$  from 1.0 to 1.2 V clearly demonstrate a voltage-tunable,

bright, nanoscale light source (diffraction limited). Figure 1c shows a representative light emission spectrum recorded for a Au junction (zero-bias dc conductance  $G = 0.25 G_0$ , where  $G_0 = 2e^2/h$  is the conductance quantum). Note that all light recorded by the spectrometer are above-threshold ( $\hbar\omega > 1\ \text{eV}$ ). Furthermore, we performed polarization-dependent measurements of the light emission to examine the plasmonic modes of the tunnel junction. A polarizer is placed right in front of the CCD spectrometer to directly obtain the polarization information on the emitted light. As shown in Figure 1d, the polarization-spectral contour plot reveals the mode structure of the LSP resonances excited by the inelastic tunneling electrons, with emission peaks at  $\sim 1.3$  and  $1.7\ \text{eV}$  for the studied junction (see also in Figure 1c). Past studies<sup>33</sup> on the plasmonic properties of such tunnel junction devices have shown that both the dipolar “tip” plasmons and transverse plasmons originating from the nanowire contribute to the plasmonic modes. The hybridization of these and higher order multipolar modes due to the broken symmetry of the tunnel junction geometry creates the LSPs in the gap.

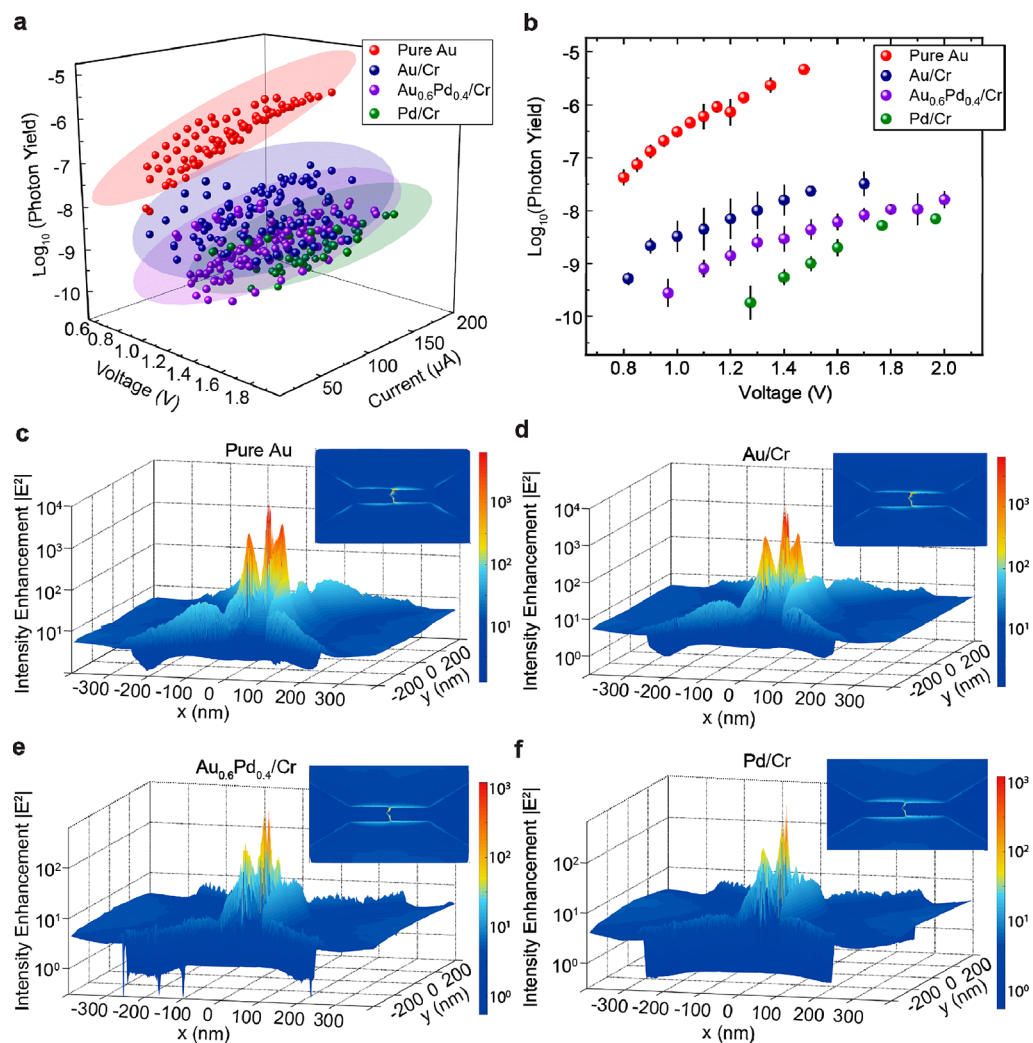


**Figure 3.** Measured material- and voltage-dependence of above-threshold light emission and numerical simulations of the radiative field enhancement due to localized plasmons in the tunneling gap. (a) Measured photon yield (plotted on logarithmic scale) for  $\sim 100$  tunnel junction devices made of different materials versus applied voltage and tunneling current. The ellipsoids correspond to a 95% confidence interval fit to the experimental data. (b) Measured photon yield versus applied voltage for the ensemble of selected devices with tunneling current of  $\sim 100 \mu\text{A}$ . Error bars are the standard deviation over the measured junctions for each material at each bias. (c) Finite-element simulation results of plasmon-induced electric field intensity enhancement (proportional to the local photon density of states in the gap) at 785 nm (corresponds to the peak wavelength of the observed light emission) for the Au junction. The insets show the top-view of the 3D plots, indicating the geometry of the simulated junction and the 2D intensity. (d–f) Same as (c), but for junctions made of other materials. The field enhancement is seen to be smaller than that in (c).

We further examined in detail the above-threshold light emission in tunnel junctions under different driving voltages and tunneling current. As shown in Figure 2, we performed light emission measurement on the same tunnel junctions in high- and low-current regimes. To elaborate, as described above, controlled electromigration was applied to break the nanowire to form a tunneling gap. After the experiment was done, the same junction was electromigrated further, by applying a higher voltage to form a larger separation gap which is indicated by a much smaller zero-bias conductance compared to the tunnel junction before the second electromigration. The tunnel junctions after the first and second electromigration step were oftenly found to allow a high ( $\sim 100 \mu\text{A}$ ) and low (below  $10 \mu\text{A}$ ) tunneling current, respectively.

Comparison of the results from Au/Cr and pure Au junctions reveals important insights. In Au/Cr junctions, light emission in high-current regime (Figure 2a) contains a substantial above-threshold portion, whereas the same device

in low-current regime (Figure 2b) exhibits a clear energy cutoff at  $eV$ , reminiscent of the previous studies of below-threshold light emission.<sup>9,13,18</sup> In contrast, in the pure Au junction, high-current regime (Figure 2c) shows that all photons have energies exceeding the  $eV$  threshold. Moreover, in low-current regime (Figure 2d), above-threshold photons are still observable (different from that in Figure 2b for the same current regime), even though the tunneling current in this junction is much smaller than the Au/Cr case. Note here that since device-to-device variation in the obtained conductance of tunnel junctions is significant, it is most meaningful to compare ensembles of devices by photon yield under the same applied voltage, that is, to calculate the total emitted photons per tunneling electrons. We define photon yield  $Q$  as  $U/I$ , where  $U$  is the total photon counts and  $I$  is the tunneling current. Interestingly, the enhancement factor  $Q_{\text{high}}/Q_{\text{low}}$  between the high- and low-current regime is found to be always larger than 1 (see Supporting Information Section 4 and Figure S3 for

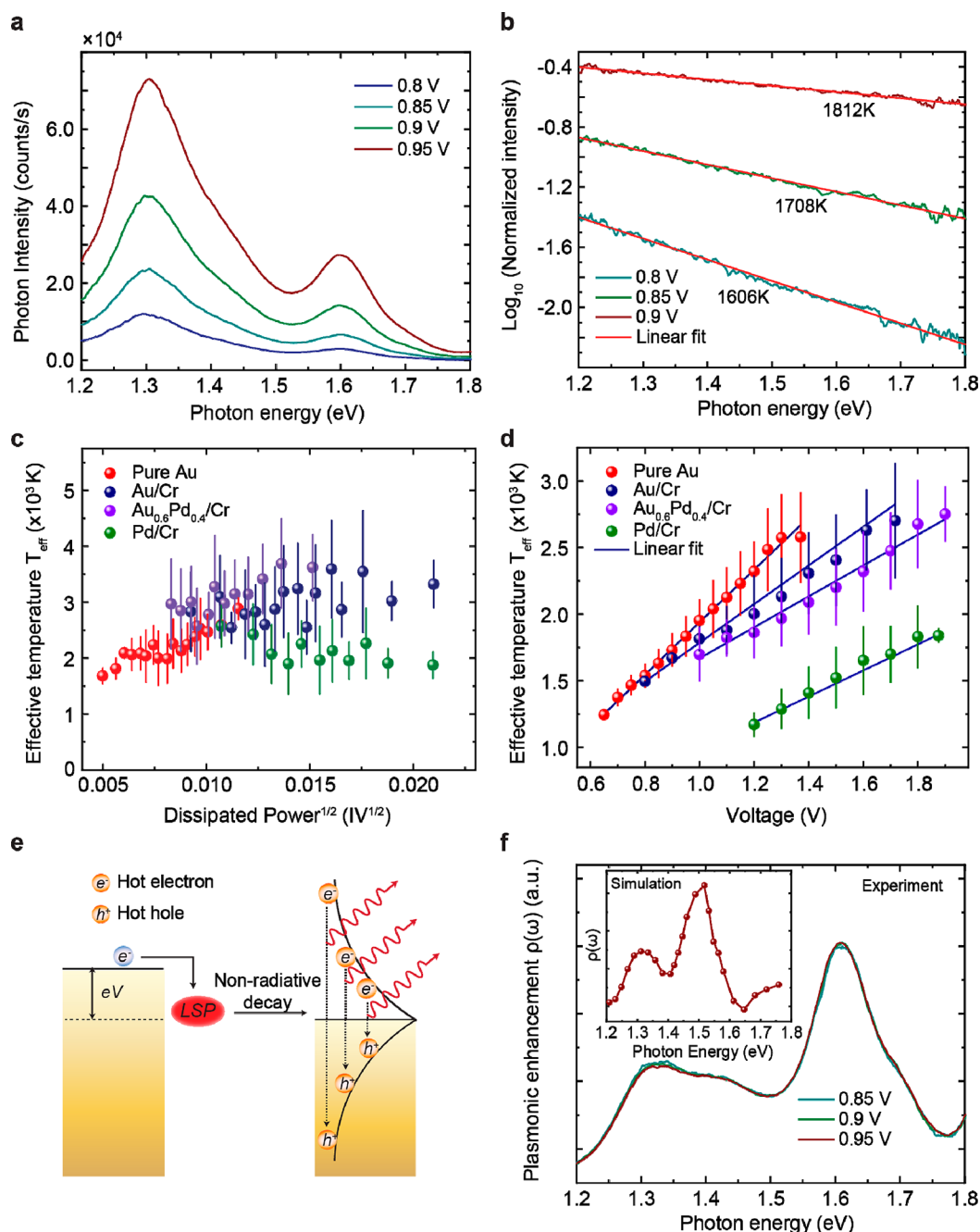


**Figure 4.** Analysis and theoretical model of above-threshold light emission in tunnel junctions. (a) Measured light emission from a Au junction under different voltage. (b) Normalization analysis of the spectra in (a), by dividing the measured spectrum at 0.8, 0.85, and 0.9 V with reference to the spectrum at 0.95 V. The linear decay of the normalized spectra (on logarithmic scale) is fitted to a Boltzmann energy distribution  $e^{-h\omega/k_B T_{\text{eff}}}$  (solid red lines), where  $T_{\text{eff}}$  is the effective temperature of hot carriers (electrons and holes). (c) Statistical analysis over a large ensemble of junctions on the extracted  $T_{\text{eff}}$  of hot carriers as a function of power dissipation ( $(IV)^{1/2}$ ) in the junctions for different materials. It can be seen that  $T_{\text{eff}}$  is relatively independent of the dissipated power, even within a single material. (d) Statistical analysis on  $T_{\text{eff}}$  as a function of applied voltage (V). The solid lines are the best linear fit to the data. Error bars are the standard deviation over the ensemble of junctions for each material at the applied voltage. (e) Schematics of the theoretical model in which light emission comes from the radiative recombination of hot electrons and holes, which is sustained in a steady-state distribution during the continuous electrical excitations of LSPs in the junction. (f) Extracted voltage-independent spectral plasmonic enhancement,  $\rho(\omega)$ , due to LSPs in the tunnel junction from applying eq 2. Inset shows the numerically calculated plasmonic enhancement for a tunnel junction with a similar geometry.

more results from  $\sim 30$  junctions), indicating a nonlinear relation between the above-threshold light emission and tunneling current.

To understand the observed material-dependent characteristics of above-threshold light emission and the photon yield in Figure 2, we then conducted systematic measurements on over

100 devices made of different materials under a series of voltages and tunneling currents. Figure 3a summarizes the results by plotting photon yield (on logarithmic scale) as a function of the applied voltage and the corresponding tunneling current. It is clearly seen that pure Au junctions

feature the highest photon yield, followed by Au/Cr, Au<sub>0.6</sub>Pd<sub>0.4</sub>/Cr, and Pd/Cr with the lowest yield.

We can proceed further and select a set of junctions with roughly similar tunneling current ( $\sim 100 \mu\text{A}$ , at which level above-threshold light emission was observed for all materials). The purpose of such selection is to examine the relationship between photon yield and applied voltage, excluding the effect of tunneling current. As shown below in our theoretical model, this relationship is critical to reveal the physical origin of above-threshold photon emission. As shown in Figure 3b, we found that under the same applied voltage and current the photon yield of pure Au junctions is around 2 to 3 orders of magnitude higher than Au/Cr and Au<sub>0.6</sub>Pd<sub>0.4</sub>/Cr junctions, and nearly 4 orders of magnitude higher than Pd/Cr junctions. While one may expect a larger photon yield from a good plasmonic material such as pure Au compared to a well-known poor plasmonic material such as Pd and Pd/Cr (with Cr further attenuating the plasmonic response of Pd), the observation of orders-of-magnitude material-dependent discrepancy is surprising.

To show that, plasmon-induced radiative field enhancement (a direct indicator of the strength of the plasmonic resonances) can be inferred directly from the calculation of the electrical field intensity within the tunneling gap (see Supporting Information Section 5 and Figure S3 for details of our finite-element modeling and more results). The quality of a plasmonic material can be quantified by its plasmonicity<sup>34</sup> and is mainly determined by the imaginary part of the relative permittivity. The permittivities at 785 nm are Au,<sup>35</sup>  $-22.855 + 1.4245i$ ; Cr,<sup>36</sup>  $-2.0612 + 21.601i$ ; and Pd,<sup>36</sup>  $-21.243 + 20.086i$ , clearly showing the superiority of Au as a plasmonic material. As shown in Figure 3c–f, we found that the localized plasmons in pure Au junctions indeed lead to the highest radiative field enhancement among the studied materials but only differ from the worst plasmonic material (Pd/Cr) by a factor of  $\sim 20$ , dramatically smaller than the measured photon yield difference ( $\sim 10^4$ ) in light emission. These observations, combined with numerical simulations, strongly suggest that above-threshold light emission does not originate solely from a simple plasmonic field enhancement effect due to LSPs in the gap.

In analogy with prior efforts,<sup>25,26</sup> we performed a normalization analysis on the measured light emission spectra under different voltages by dividing with reference to the spectrum obtained at the highest voltage. The normalization separates the contributions of voltage-independent plasmonic resonances of the tunnel junction, which depends only on junction geometry and the material type, from the voltage-dependent component of observed light emission. Representative measurement results of light emission from a typical Au tunnel junction at 0.8, 0.85, 0.9, and 0.95 V are shown in Figure 4a. After spectral normalization, the reduced emission spectra are plotted in Figure 4b, which demonstrates that the normalized spectra intensity, on logarithmic scale, decays linearly with the photon energy (see Supporting Information Sections 6 and 7 for more results on different materials and at different substrate temperatures).

This energy dependence of light emission can then be described phenomenologically by a Boltzmann statistics factor  $e^{-\hbar\omega/k_{\text{B}}T_{\text{eff}}}$ , where  $T_{\text{eff}}$  is an effective temperature of the hot carriers, out of equilibrium with the lattice and the background of cold electrons. Proper caution is needed to introduce the concept of effective temperature in any driven, nonequilibrium

system.<sup>37,38</sup> In this case, the clear linearity of Figure 4b shows that an effective Boltzmann factor describes the hot carrier distribution, as in past studies.<sup>39–41</sup> When the typical time interval between tunneling events (on the order of tens of femtoseconds for large currents) is much smaller than the relaxation time of the hot carriers (about a few hundreds of femtoseconds to picoseconds), hot carriers generated by the electrically excited plasmons will undergo many scattering events, forming a nonthermal steady-state distribution, before thermalizing into the lattice phonons.<sup>42</sup> The steady-state distribution can then be parametrized using an effective temperature.

We extracted the effective temperature  $T_{\text{eff}}$  from the normalized emission spectra in Figure 4b by fitting with a Boltzmann factor. It can be seen that  $T_{\text{eff}}$  reaches over 1000 K, much higher than the equilibrium lattice temperature of the junction (i.e., the 5 K substrate temperature). It appears that above-threshold emission originates from hot carriers. These findings raise the questions: What is the physical explanation of very high nonequilibrium  $T_{\text{eff}}$ ? What are the factors determining  $T_{\text{eff}}$  in such plasmonic systems?

To address these questions, we applied the normalization analysis described above to measure emission spectra from the large ensemble of tunnel junctions. To identify the relationship between  $T_{\text{eff}}$  and the applied electrical condition (voltage or tunneling current), we evaluate two candidate families of models,  $T_{\text{eff}} \propto \sqrt{P} = \sqrt{IV}$  and  $T_{\text{eff}} \propto V$ , where  $P$  is the dissipated power in the junction. Briefly, the first approach is based on the hypothesis that  $T_{\text{eff}}$  of hot electrons in the tunnel junction is determined by the electrical power dissipation and coupling between the charge carriers and lattice phonons.<sup>25</sup> In this “thermal” model, the blackbody radiation of the hot-electron gas generates broadband above-threshold photons. The second approach considers the electrically driven generation and relaxation of plasmon-induced hot carriers (see below for our microscopic theoretical model).

The results of statistical analysis across the large ensemble of junctions for the first approach is summarized in Figure 4c. We find that  $T_{\text{eff}}$  inferred from the normalized emission is largely uncorrelated with the dissipated electrical power for each of materials studied here. Instead, as shown in Figure 4d, a linear relationship between  $T_{\text{eff}}$  and the applied voltage is clearly indicated. Moreover, materials with less plasmonic loss exhibit higher  $T_{\text{eff}}$  at a given voltage, providing further evidence that plasmons play a key role in the generation of the hot carriers.

Having established empirical correlation between  $T_{\text{eff}}$  and  $V$  directly from our experimental analysis, we sketch a physical model (see schematics in Figure 4e and detailed derivation of our model in Supporting Information Section 8) to understand this relationship, as well as the generation of above-threshold photons due to plasmon-induced hot-carrier dynamics. While a realistic quantitative theory is extremely challenging, this toy model attempts to capture the essential physics of electrically driven process of hot carrier generation and relaxation. Optical excitation only induces interactions with bright dipolar plasmons. In contrast, inelastic tunneling electrons can excite any localized plasmon (dark and bright) in the tunnel junction.<sup>43</sup> LSPs excited by inelastic tunneling electrons undergo a nonradiative decay process in which a plasmon energy quantum  $\hbar\omega_{\text{LSP}}$  is transferred to an individual conduction hot electron–hole pair. The energy distribution of these hot carriers is centered around the Fermi level  $\epsilon_{\text{F}}$  and extends to  $\epsilon_{\text{F}} \pm eV$ . If the rate of tunneling events outpaces

carrier relaxation, a steady-state hot carrier distribution is sustained, with its specific form depending on the time interval between successive electron tunneling events ( $\propto e/I$ ) and the hot carrier lifetimes (approximately hundreds of femtoseconds).<sup>6</sup> The above-threshold light emission originates from the plasmon-enhanced radiative recombination of hot electrons and holes with high energies in the hot-carrier distribution.

In this picture, a prediction is that a steady-state effective temperature of the hot carriers is directly correlated with the bias window ( $eV$ ) applied to drive the plasmonic process, rather than the dissipated electrical power. Specifically, we found that

$$k_{\text{B}}T_{\text{eff}} \propto \beta eV \quad (1)$$

where  $\beta$  is material-dependent parameter correlated with the quality of plasmonic response of a material. Equation 1 agrees very well with our experimental observation in Figure 4d at sufficiently large voltage, and likewise is consistent with the difference in  $T_{\text{eff}}$  found between plasmonically active and lossy materials at the same voltage (see Figure S6). In fact, the dielectric function of transition metals such as Cr and Pd in this energy range dampens the LSPs, thereby decreasing the generation rate of hot carriers through this inelastic excitation mechanism. In addition, the unfilled  $d$ -band increases the electronic density of states around  $\varepsilon_{\text{F}}$ , thereby decreasing the lifetimes of excited carriers. This shifts the steady-state distribution to the lower energies (closer to  $\varepsilon_{\text{F}}$ ), making above-threshold light emission less likely.<sup>6</sup>

Beyond this simple model, we note that a more detailed treatment of this problem looking at the redistribution of energy within the electronic system as a consequence of the viscosity of the electron liquid, predicts the same voltage dependence of the effective carrier temperature<sup>44</sup> in a point-contact geometry similar to that here. The material dependence in that approach would result from the role of (material-dependent) LSPs in enhancing the effective frictional heating of the electronic fluid.

With the insight from this greatly simplified model, a physical picture of the above-threshold light emission can then be obtained. We consider the spectral intensity of the light emission

$$U(\omega) \approx \rho(\omega)I^{\alpha}\hbar\omega e^{-\hbar\omega/k_{\text{B}}T_{\text{eff}}} \quad (2)$$

where  $\rho(\omega)$  is the local photon density of states (which gives the radiative field enhancement effect due to LSPs for a given junction),  $\alpha$  indicates the nonlinear tunneling current-dependence of the above-threshold light emission. The value of  $\alpha$ , always greater than 1, is obtained from the experimental results (see Supporting Information Section 4). We note that eq 2 is inspired by the hot carrier model<sup>39,45</sup> to explain anti-Stokes photoluminescence in plasmonic nanoparticles, which, phenomenologically similar to the observed above-threshold light emission, involves photon emission with energies above that of the excited photons (rather than incident electrons studied here). The observed anti-Stokes photoluminescence has been understood as either plasmon-enhanced electron–hole generation and recombination, or Raman scattering from the intraband electronic continuum.<sup>46–48</sup>

Using eq 2, combined with the inferred value of  $T_{\text{eff}}$  from the normalization analysis, our analysis permits the extraction of  $\rho(\omega)$ . As shown in Figure 4f, this spectrum shows good

qualitative consistency with the electrical field intensity enhancement as a function of photon energy calculated (inset of Figure 4f) by the finite-element modeling of the plasmonic resonances for a typical device geometry.

The remarkable dependence of photon yield on the plasmonic properties of the constituent metal, a factor of  $10^4$  between pure Au and Pd/Cr devices, shows that plasmons play a larger role in the process than just modifying optical density of states  $\rho(\omega)$ . We found clear evidence that plasmon-enhanced hot carrier dynamics are central in the generation of above-threshold photons and are responsible for the observed dramatic yield discrepancy among metallic materials. While a rigorous treatment of this nonequilibrium, open-system problem involving atomic-scale interelectrode distances would require detailed electronic structure calculations, the overall material dependence is strongly influenced by the metal dielectric (and hence plasmonic) response. Our observations and analysis show that hot-carrier distributions with effective temperatures (above 2000 K) are achievable under modest electrical bias ( $\sim 1$  V) in properly designed plasmonic nanostructures, opening avenues for optimization and possible utility in plasmonic chemistry<sup>19</sup> and optoelectronic applications. Similarly, the large plasmonic enhancement of light emission raises possibilities for nontrivial quantum optical effects, as have been seen in other subnanometer plasmonic gap systems.<sup>49</sup>

## ■ ASSOCIATED CONTENT

### Supporting Information

The Supporting Information is available free of charge at <https://pubs.acs.org/doi/10.1021/acs.nanolett.0c02121>.

Device nanofabrication; electromigration break junction protocol; experimental setup; evaluation of tunneling current dependence of light emission; finite-element modeling; additional normalization analysis results in different materials; influence of substrate temperature on above-threshold light emission; theoretical model (PDF)

## ■ AUTHOR INFORMATION

### Corresponding Author

**Douglas Natelson** – Department of Physics and Astronomy and Smalley-Curl Institute, Department of Electrical and Computer Engineering, and Department of Materials Science and Nanoengineering, Rice University, Houston, Texas 77005, United States; [orcid.org/0000-0003-2370-9859](https://orcid.org/0000-0003-2370-9859); Email: [natelson@rice.edu](mailto:natelson@rice.edu)

### Authors

**Longji Cui** – Department of Physics and Astronomy and Smalley-Curl Institute, Rice University, Houston, Texas 77005, United States; Department of Mechanical Engineering and Materials Science and Engineering Program, University of Colorado, Boulder, Colorado 80309, United States; [orcid.org/0000-0003-0469-3230](https://orcid.org/0000-0003-0469-3230)

**Yunxuan Zhu** – Department of Physics and Astronomy and Smalley-Curl Institute, Rice University, Houston, Texas 77005, United States

**Mahdiyeh Abbasi** – Department of Electrical and Computer Engineering, Rice University, Houston, Texas 77005, United States

**Arash Ahmadivand** – Department of Electrical and Computer Engineering, Rice University, Houston, Texas 77005, United States; [orcid.org/0000-0003-0808-8775](https://orcid.org/0000-0003-0808-8775)

**Burak Gerislioglu** – Department of Physics and Astronomy and Smalley-Curl Institute, Rice University, Houston, Texas 77005, United States; [orcid.org/0000-0001-8575-7990](https://orcid.org/0000-0001-8575-7990)

**Peter Nordlander** – Department of Physics and Astronomy and Smalley-Curl Institute, Department of Electrical and Computer Engineering, and Department of Materials Science and Nanoengineering, Rice University, Houston, Texas 77005, United States; [orcid.org/0000-0002-1633-2937](https://orcid.org/0000-0002-1633-2937)

Complete contact information is available at:

<https://pubs.acs.org/10.1021/acs.nanolett.0c02121>

### Author Contributions

D.N. and L.C. designed the experiment. L.C. and Y.Z. fabricated the devices, conducted the transport and light emission experiment, and theoretically modeled the data. M.A. performed the finite-element numerical simulation. P.N. analytically modeled the driven hot carrier system. A.A. and B.G. performed additional modeling. L.C., D.N., and P.N. wrote the manuscript with comments and inputs from all authors. All authors have given approval to the final version of the manuscript.

### Funding

NSF ECCS-1704625, Robert A. Welch Foundation award C-1222 and C-1636, and AFOSR award No. FA 9550-15-1-0022.

### Notes

The authors declare no competing financial interest.

### ACKNOWLEDGMENTS

The authors acknowledge M. Di Ventra for insightful conversations. L.C. acknowledges funding support from J. Evans Attwell Welch Fellowship, the Smalley Curl Institute at Rice University, and support from the University of Colorado Boulder. D.N. and Y.Z. acknowledge Robert A. Welch Foundation award C-1636. D.N. and M.A. acknowledge support for modelling from NSF ECCS-1704625. P.N. acknowledges Robert A. Welch Foundation award C-1222 and AFOSR award No. FA 9550-15-1-0022.

### ABBREVIATIONS

LSP, localized surface plasmon

### REFERENCES

- (1) Christopher, P.; Xin, H. L.; Linic, S. Visible-light-enhanced catalytic oxidation reactions on plasmonic silver nanostructures. *Nat. Chem.* **2011**, *3* (6), 467–472.
- (2) Cortés, E.; Xie, W.; Cambiasso, J.; Jermyn, A. S.; Sundaraman, R.; Narang, P.; Schlücker, S.; Maier, S. A. Plasmonic hot electron transport drives nano-localized chemistry. *Nat. Commun.* **2017**, *8* (1), 14880.
- (3) Zhou, L.; Swearer, D. F.; Zhang, C.; Robotjazi, H.; Zhao, H. Q.; Henderson, L.; Dong, L. L.; Christopher, P.; Carter, E. A.; Nordlander, P.; Halas, N. J. Quantifying hot carrier and thermal contributions in plasmonic photocatalysis. *Science* **2018**, *362* (6410), 69–72.
- (4) Knight, M. W.; Sobhani, H.; Nordlander, P.; Halas, N. J. Photodetection with Active Optical Antennas. *Science* **2011**, *332* (6030), 702–704.
- (5) Li, W.; Coppens, Z. J.; Besteiro, L. V.; Wang, W. Y.; Govorov, A. O.; Valentine, J. Circularly polarized light detection with hot electrons in chiral plasmonic metamaterials. *Nat. Commun.* **2015**, *6*, 8379.

- (6) Cai, Y. Y.; Liu, J. G.; Tauzin, L. J.; Huang, D.; Sung, E.; Zhang, H.; Joplin, A.; Chang, W. S.; Nordlander, P.; Link, S. Photoluminescence of Gold Nanorods: Purcell Effect Enhanced Emission from Hot Carriers. *ACS Nano* **2018**, *12* (2), 976–985.

- (7) Green, M. A.; Pillai, S. Harnessing plasmonics for solar cells. *Nat. Photonics* **2012**, *6* (3), 130–132.

- (8) Atwater, H. A.; Polman, A. Plasmonics for improved photovoltaic devices. *Nat. Mater.* **2010**, *9* (3), 205–213.

- (9) Kern, J.; Kulloock, R.; Prangma, J.; Emmerling, M.; Kamp, M.; Hecht, B. Electrically driven optical antennas. *Nat. Photonics* **2015**, *9* (9), 582–586.

- (10) Dasgupta, A.; Mennemanteuil, M. M.; Buret, M.; Cazier, N.; Colas-Des-Francis, G.; Bouhelier, A. Optical wireless link between a nanoscale antenna and a transducing rectenna. *Nat. Commun.* **2018**, *9* (1), 1992.

- (11) Kullock, R.; Ochs, M.; Grimm, P.; Emmerling, M.; Hecht, B. Electrically-driven Yagi-Uda antennas for light. *Nat. Commun.* **2020**, *11* (1), 115.

- (12) Leon, C. C.; Roslowska, A.; Grewal, A.; Gunnarsson, O.; Kuhnke, K.; Kern, K. Photon superbunching from a generic tunnel junction. *Sci. Adv.* **2019**, *5* (5), No. eaav4986.

- (13) Parzefall, M.; Bharadwaj, P.; Jain, A.; Taniguchi, T.; Watanabe, K.; Novotny, L. Antenna-coupled photon emission from hexagonal boron nitride tunnel junctions. *Nat. Nanotechnol.* **2015**, *10* (12), 1058–1063.

- (14) Du, W.; Wang, T.; Chu, H. S.; Wu, L.; Liu, R. R.; Sun, S.; Phua, W. K.; Wang, L. J.; Tomczak, N.; Nijhuis, C. A. On-chip molecular electronic plasmon sources based on self-assembled monolayer tunnel junctions. *Nat. Photonics* **2016**, *10* (4), 274–280.

- (15) Harutyunyan, H.; Martinson, A. B. F.; Rosenmann, D.; Khorashad, L. K.; Besteiro, L. V.; Govorov, A. O.; Wiederrecht, G. P. Anomalous ultrafast dynamics of hot plasmonic electrons in nanostructures with hot spots. *Nat. Nanotechnol.* **2015**, *10* (9), 770–774.

- (16) Du, W.; Wang, T.; Chu, H. S.; Nijhuis, C. A. Highly efficient on-chip direct electronic-plasmonic transducers. *Nat. Photonics* **2017**, *11* (10), 623–627.

- (17) Lambe, J.; McCarthy, S. L. Light-Emission from Inelastic Electron-Tunneling. *Phys. Rev. Lett.* **1976**, *37* (14), 923–925.

- (18) Qian, H. L.; Hsu, S. W.; Gurunatha, K.; Riley, C. T.; Zhao, J.; Lu, D.; Tao, A. R.; Liu, Z. W. Efficient light generation from enhanced inelastic electron tunnelling. *Nat. Photonics* **2018**, *12* (8), 485–488.

- (19) Wang, P.; Krasavin, A. V.; Nasir, M. E.; Dickson, W.; Zayats, A. V. Reactive tunnel junctions in electrically driven plasmonic nanorod metamaterials. *Nat. Nanotechnol.* **2018**, *13* (2), 159–164.

- (20) Zhang, C.; Hugonin, J. P.; Coutrot, A. L.; Sauvan, C.; Marquier, F.; Greffet, J. J. Antenna surface plasmon emission by inelastic tunneling. *Nat. Commun.* **2019**, *10* (1), 4949.

- (21) Gurunathan, S. P.; Verellen, N.; Zharinov, V. S.; Shirley, F. J.; Moshchalkov, V. V.; Heyns, M.; Van de Vondel, J.; Radu, I. P.; Van Dorpe, P. Electrically Driven Unidirectional Optical Nanoantennas. *Nano Lett.* **2017**, *17* (12), 7433–7439.

- (22) Downes, A.; Dumas, P.; Welland, M. E. Measurement of high electron temperatures in single atom metal point contacts by light emission. *Appl. Phys. Lett.* **2002**, *81* (7), 1252–1254.

- (23) Hoffmann, G.; Berndt, R.; Johansson, P. Two-electron photon emission from metallic quantum wells. *Phys. Rev. Lett.* **2003**, *90* (4), 046803.

- (24) Pechou, R.; Coratger, R.; Ajustron, F.; Beauvillain, J. Cutoff anomalies in light emitted from the tunneling junction of a scanning tunneling microscope in air. *Appl. Phys. Lett.* **1998**, *72* (6), 671–673.

- (25) Buret, M.; Uskov, A. V.; Dellinger, J.; Cazier, N.; Mennemanteuil, M. M.; Berthelot, J.; Smetanin, I. V.; Protsenko, I. E.; Colas-Des-Francis, G.; Bouhelier, A. Spontaneous Hot-Electron Light Emission from Electron-Fed Optical Antennas. *Nano Lett.* **2015**, *15* (9), 5811–5818.

- (26) Peters, P. J.; Xu, F.; Kaasbjerg, K.; Rastelli, G.; Belzig, W.; Berndt, R. Quantum Coherent Multielectron Processes in an Atomic Scale Contact. *Phys. Rev. Lett.* **2017**, *119* (6), 066803.

- (27) Schull, G.; Neel, N.; Johansson, P.; Berndt, R. Electron-Plasmon and Electron-Electron Interactions at a Single Atom Contact. *Phys. Rev. Lett.* **2009**, *102* (5), 057401.
- (28) Xu, F.; Holmqvist, C.; Belzig, W. Overbias Light Emission due to Higher-Order Quantum Noise in a Tunnel Junction. *Phys. Rev. Lett.* **2014**, *113* (6), 066801.
- (29) Kaasbjerg, K.; Nitzan, A. Theory of Light Emission from Quantum Noise in Plasmonic Contacts: Above-Threshold Emission from Higher-Order Electron-Plasmon Scattering. *Phys. Rev. Lett.* **2015**, *114* (12), 126803.
- (30) Aouani, H.; Wenger, J.; Gerard, D.; Rigneault, H.; Devaux, E.; Ebbesen, T. W.; Mahdavi, F.; Xu, T. J.; Blair, S. Crucial Role of the Adhesion Layer on the Plasmonic Fluorescence Enhancement. *ACS Nano* **2009**, *3* (7), 2043–2048.
- (31) Habteyes, T. G.; Dhuey, S.; Wood, E.; Gargas, D.; Cabrini, S.; Schuck, P. J.; Alivisatos, A. P.; Leone, S. R. Metallic Adhesion Layer Induced Plasmon Damping and Molecular Linker as a Nondamping Alternative. *ACS Nano* **2012**, *6* (6), 5702–5709.
- (32) Park, H.; Lim, A. K. L.; Alivisatos, A. P.; Park, J.; McEuen, P. L. Fabrication of metallic electrodes with nanometer separation by electromigration. *Appl. Phys. Lett.* **1999**, *75* (2), 301–303.
- (33) Herzog, J. B.; Knight, M. W.; Li, Y.; Evans, K. M.; Halas, N. J.; Natelson, D. Dark Plasmons in Hot Spot Generation and Polarization in Interelectrode Nanoscale Junctions. *Nano Lett.* **2013**, *13* (3), 1359–1364.
- (34) Zhang, R.; Bursi, L.; Cox, J. D.; Cui, Y.; Krauter, C. M.; Alabastri, A.; Manjavacas, A.; Calzolari, A.; Corni, S.; Molinari, E.; Carter, E. A.; García de Abajo, F. J.; Zhang, H.; Nordlander, P. How To Identify Plasmons from the Optical Response of Nanostructures. *ACS Nano* **2017**, *11* (7), 7321–7335.
- (35) Johnson, P. B.; Christy, R. W. Optical Constants of Noble Metals. *Phys. Rev. B* **1972**, *6* (12), 4370–4379.
- (36) Johnson, P. B.; Christy, R. W. Optical constants of transition metals: Ti, V, Cr, Mn, Fe, Co, Ni, and Pd. *Phys. Rev. B* **1974**, *9* (12), 5056–5070.
- (37) Dubi, Y.; Di Ventra, M. Colloquium: Heat flow and thermoelectricity in atomic and molecular junctions. *Rev. Mod. Phys.* **2011**, *83* (1), 131–155.
- (38) Zhang, D.; Zheng, X.; Di Ventra, M. Local temperatures out of equilibrium. *Phys. Rep.* **2019**, *830*, 1–66.
- (39) Cai, Y. Y.; Sung, E.; Zhang, R. M.; Tauzin, L. J.; Liu, J. G.; Ostovar, B.; Zhang, Y.; Chang, W. S.; Nordlander, P.; Link, S. Anti-Stokes Emission from Hot Carriers in Gold Nanorods. *Nano Lett.* **2019**, *19* (2), 1067–1073.
- (40) Szczerbinski, J.; Gyr, L.; Kaeslin, J.; Zenobi, R. Plasmon-Driven Photocatalysis Leads to Products Known from E-beam and X-ray-Induced Surface Chemistry. *Nano Lett.* **2018**, *18* (11), 6740–6749.
- (41) He, Y. B.; Xia, K. Y.; Lu, G. W.; Shen, H. M.; Cheng, Y. Q.; Liu, Y. C.; Shi, K. B.; Xiao, Y. F.; Gong, Q. H. Surface enhanced anti-Stokes one-photon luminescence from single gold nanorods. *Nano-scale* **2015**, *7* (2), 577–582.
- (42) Liu, J. G.; Zhang, H.; Link, S.; Nordlander, P. Relaxation of Plasmon-Induced Hot Carriers. *ACS Photonics* **2018**, *5* (7), 2584–2595.
- (43) de Abajo, F. J. G. Optical excitations in electron microscopy. *Rev. Mod. Phys.* **2010**, *82* (1), 209–275.
- (44) D'Agosta, R.; Sai, N.; Di Ventra, M. Local Electron Heating in Nanoscale Conductors. *Nano Lett.* **2006**, *6* (12), 2935–2938.
- (45) Carattino, A.; Caldarola, M.; Orrit, M. Gold Nanoparticles as Absolute Nanothermometers. *Nano Lett.* **2018**, *18* (2), 874–880.
- (46) Mertens, J.; Kleemann, M.-E.; Chikkaraddy, R.; Narang, P.; Baumberg, J. J. How Light Is Emitted by Plasmonic Metals. *Nano Lett.* **2017**, *17* (4), 2568–2574.
- (47) Hugall, J. T.; Baumberg, J. J. Demonstrating Photo-luminescence from Au is Electronic Inelastic Light Scattering of a Plasmonic Metal: The Origin of SERS Backgrounds. *Nano Lett.* **2015**, *15* (4), 2600–2604.
- (48) Huang, J.; Wang, W.; Murphy, C. J.; Cahill, D. G. Resonant secondary light emission from plasmonic Au nanostructures at high electron temperatures created by pulsed-laser excitation. *Proc. Natl. Acad. Sci. U. S. A.* **2014**, *111* (3), 906–911.
- (49) Benz, F.; Schmidt, M. K.; Dreismann, A.; Chikkaraddy, R.; Zhang, Y.; Demetriadou, A.; Carnegie, C.; Ohadi, H.; de Nijs, B.; Esteban, R.; Aizpurua, J.; Baumberg, J. J. Single-molecule optomechanics in “picocavities. *Science* **2016**, *354* (6313), 726–729.